GeoHazards

Article

Modelling and Validation of the Derna Dam Break Event

Alessandro Annunziato [1,*], Marzia Santini [2], Chiara Proietti [3], Ludovica de Girolamo [4], Valerio Lorini [2], Andrea Gerhardinger [3] and Michele Tucci [3]

1 Independent Researcher, 21020 Taino, VA, Italy
2 Joint Research Centre of the European Commission, 21027 Ispra, VA, Italy; marzia.santini@ec.europa.eu (M.S.); valerio.lorini@europarl.europa.eu (V.L.)
3 FINCONS SPA, 20871 Vimercate, MB, Italy; chiara.proietti@ext.ec.europa.eu (C.P.); andrea.gerhardinger@ext.ec.europa.eu (A.G.); michele.tucci@ext.ec.europa.eu (M.T.)
4 Seidor Italy SRL, 20129 Milano, MI, Italy; ludovica.de-girolamo@ext.ec.europa.eu
* Correspondence: alessandro.annunziato@gmail.com

Abstract: The catastrophic failure of two dams in Libya on 10 and 11 September 2023 resulted in the devastating flooding of the city of Derna, which is located downstream of the dams, causing more than 6000 fatalities and displacing thousands of residents. The failure was attributed to heavy rainfall from Storm Daniel, leading to the dams reaching full capacity and subsequently overflowing and failing. This paper presents an analysis of the dam break, including the modelling of flow discharge and the resulting flooding of Derna. For validation purposes, this study compares the modelled quantities with post-event satellite imagery from UNOSAT and Copernicus, local reports, and data collected from social media using AI detection. The findings provide valuable insights into the dynamics of the dam break and its initial parameters, as well as an assessment of the accuracy of the results. The analysis is performed using a rapid estimation technique developed by JRC to provide the international emergency community with a swift overview of the impact and damage assessment of potential or actual dam break events. The use of all available data shows a satisfactory comparison with the calculated quantities. The rapid modelling of dam break events and combined analysis of multiple data types are proven suitable for promptly assessing the expected dynamic of the event, as well as reconstructing the unknown initial conditions before the break. Incorporating sensitivity analyses provides an estimate of the uncertainties associated with the deduced values of the unknown parameters and their relative importance in the analysis.

Keywords: dam; dam break; flooding; modelling; early warning systems; digital elevation model; population density; remote sensing

Citation: Annunziato, A.; Santini, M.; Proietti, C.; de Girolamo, L.; Lorini, V.; Gerhardinger, A.; Tucci, M. Modelling and Validation of the Derna Dam Break Event. *GeoHazards* **2024**, *5*, 504–529. https://doi.org/10.3390/geohazards5020026

Academic Editors: Mowen Xie, Yan Du, Yujing Jiang, Bo Li and Xuepeng Zhang

Received: 4 March 2024
Revised: 22 May 2024
Accepted: 22 May 2024
Published: 1 June 2024

1. Introduction

The objective of this paper is to analyse the large-scale dam break event that occurred in Libya in September 2023. This was accomplished by modelling the dam break, estimating the flood extent, establishing its timeline, and conducting a comparison of the model results with the available qualitative or quantitative post-event information.

The dam break methodology utilised in this analysis was developed by JRC and has been applied in the aftermath of recent major events or to assess potential imminent threats to infrastructure. Examples of these analyses include the failure of the dam in southern Lao People's Democratic Republic in 2018 or the potential, then actual dam break of the Nova Khavokva Dam in Ukraine in 2023. The added value of this rapid estimation approach is to provide the international emergency community with a swift overview of the damage assessment of potential or actual dam break events.

The Derna dam break provided an opportunity to validate the accuracy of the model's estimations of actual or potential damage. A comprehensive description of the methodology, including the dam break characteristics to be considered, required input quantities for the analysis, and the analytical solutions, was extensively outlined by Annunziato et al. [1].

2. Derna Dam

2.1. Storm Daniel and Dam Break Event

In September, the initial stages of the Mediterranean Cyclone (or Medicane), locally known as 'Storm Daniel', brought heavy rains to Greece, southern Bulgaria, and parts of Türkiye. The storm then remained slow-moving in the eastern Mediterranean for several days (Figure 1). On 10 and 11 September 2023, the storm's major rain bands caused extreme rainfall in northeastern Libya, with the city of Al-Bayda recording 414.1 mm in 24 h. The intense rainfall resulted in severe flooding in the region.

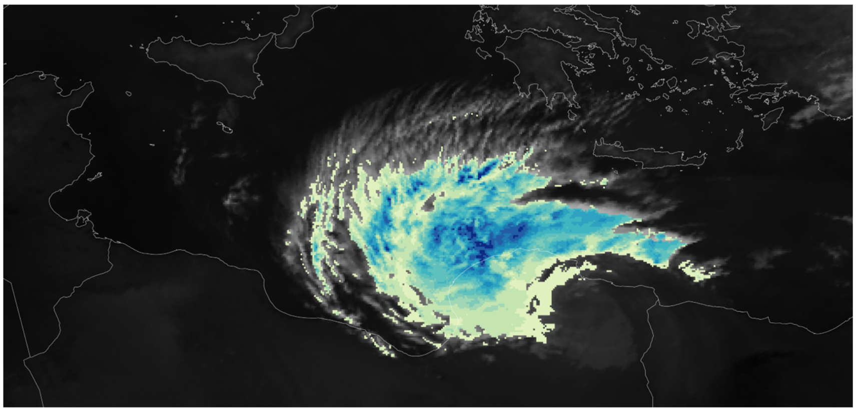

Figure 1. Satellite image showing Storm Daniel evolving in the Mediterranean Sea and affecting the northern areas of Libya (©EUMETSAT2023).

The most severe impacts were observed in the coastal city of Derna, located approximately 50 km east of Al-Bayda, where extensive flooding, exacerbated by the failure of two dams, led to the destruction of much of the city centre. As of 21 November 2023, there had been at least 4345 confirmed deaths and 8500 individuals reported as missing. Additionally, approximately 43,000 individuals were displaced across northeastern Libya due to the flooding caused by Storm Daniel [2,3] (Figure 2).

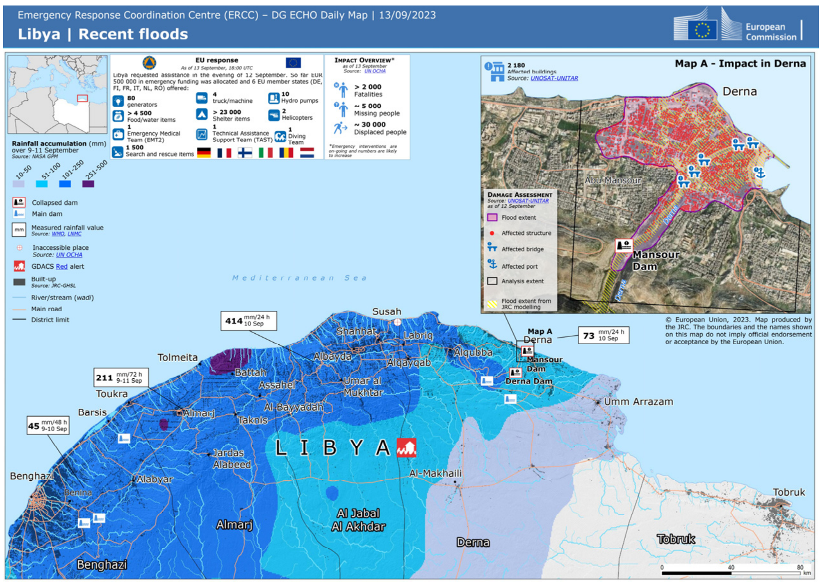

Figure 2. Situation map for the Libya floods (JRC and ECHO) [4].

Storm Daniel made landfall in Libya on 10 September, bringing strong winds and heavy rainfall. The following day, two dams located upstream of Derna collapsed under the intense pressure caused by the heavy rainfall, resulting in the release of 30 million cubic metres of water that ripped through the city (see Figure 3), home to approximately 100,000 inhabitants [2,3]. It is worth mentioning that Derna's vulnerability to flooding was well documented, as the city had previously experienced significant floods in 1942, 1959, 1968, and 1986 [5].

Figure 3. City of Derna before (left, 19 June 2023) and after (right, 13 September) the flood (©Google Earth).

The event involved two dams, as depicted in Figure 4. The Derna Dam, the larger of the two, is located approximately 12 km from the city, while the smaller Mansour Dam is situated just 1 km from the city.

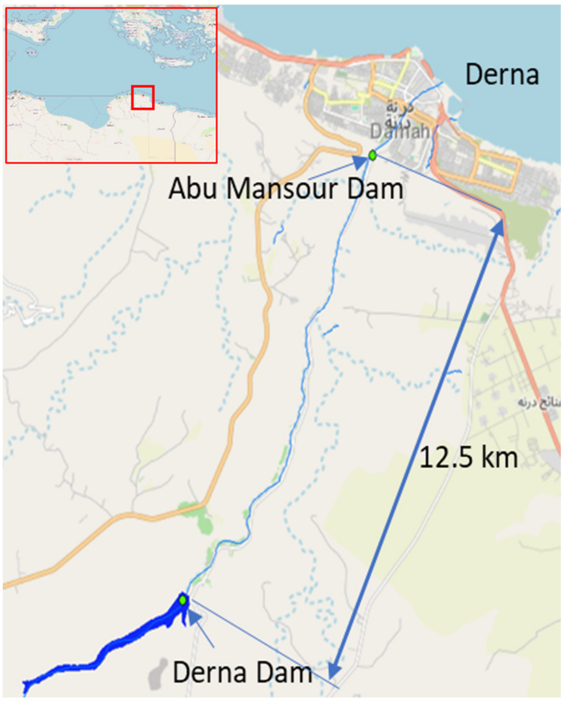

Figure 4. Geographic location of the dams with indication of approximate distance between the two (basemap from Open Street Map (OSM)).

Both dams are embankment dams with clay fill [6]. Historical imagery from Google Earth collected between 2009 and 2023 illustrates that the dams' reservoirs and the downstream river had been consistently at very low levels or completely empty. This is also confirmed by the adopted Shuttle Radar Topography Mission (SRTM) Digital Elevation Model (DEM) [7], which shows an empty riverbed upstream and downstream the dams. The sudden surge of water resulting from the intense precipitation associated with Storm

Daniel likely led to the overfilling of the Derna Dam and subsequent abrupt failure of the earth fill.

The dams were designed and constructed by the Hidroprojekt company of the former Yugoslavia Republic between 1973 and 1977. The construction of the dams aimed to facilitate irrigation of surrounding fields and to provide drinking water to Derna and nearby communities. The technical data of the dams, as per the company's website [6], are presented in Table 1; no further detail is available.

Table 1. Technical data of Derna and Mansour dams (Hidroprojekt) [6].

	Derna Dam	Mansour Dam
Dam height	75 m	45 m
Crest length	300 m	130 m
Foundation width	104 m	56 m
Embankment	735,000 m^3	104,000 m^3
Storage capacity	18 million m^3	1.5 million m^3

2.2. Previous Studies on Derna Dam

Limited studies on dam break risk assessments or specific analyses related to this event, whether published before or after the occurrence, have been identified, except for those mentioned below.

A comprehensive study conducted by Abdalla [8] focused on the potential failure of the Derna dam. In the study's abstract, the author reports the following: "*Piping failure was considered the most predictable one for Dema dam. For the current study it was shown that dam break causes a potential danger towards Dema City, since flooding occurs in the city for all hypothetical scenarios. It was recommended to predict the routing of the flow after failure due to lowering the retained water surface elevation in the reservoir and due to the use of levees and increasing walls heights in the city area*".

A relevant report by Ashoor [9] addressed potential floods in Derna caused by high precipitation. The model applied by Ashoor estimated the annual runoff volume for the study area for a forty-year period (1960–2000) to be 138.51 Mm^3. Additionally, it estimated the volume of floods based on historical events in October 1945 and late November 1986, which were associated with average precipitation of 145 mm and 64.14 mm, respectively. The 1945 rainfall resulted in a volume flood of 53.36 Mm^3, representing 40% of the annual runoff volume, while the November 1986 flood was estimated at 14.8 Mm^3, aligning well with the recorded flood in the basin. The findings underscore the high potential for flood risk in the study area, indicating the need for periodic maintenance of the dams in the Wadi Derna basin.

The European Commission Joint Research Centre (EC JRC) conducted a comprehensive analysis of the event, comparing the findings with satellite images, field reports, and social media [10].

A recent publication by Imran et al. [11] analysed the inundation of Derna following the destruction of the dam. While their results align with the findings of this study, a direct comparison with measured or observed quantities was not included.

Groenewege analysed the Derna Dam break event using Delft3D; also in this case, the author mentioned that it was used as a case study to try to understand the chain of events [12].

A further analysis of the Derna Dam break was presented by Prida [13] using the SFINCS model, taking into account different initial conditions to perform scenario analyses.

3. Methodology

3.1. Dam Break Analytical Studies vs. Rapid Analyses

The estimation of potential downstream consequences from dam-related events is an essential component of the risk assessment process implemented during the installation phase of a new dam. These calculations can be quite time-consuming and require the preparation of input decks containing all the relevant details of the dam under analysis.

However, in cases of specific ongoing or predicted natural or man-made events, there is also a need for rapid analyses that are able to provide information on areas at risk when original design analyses are unavailable or when different parameters are required. Akgun et al. [14] demonstrated the development of detailed calculations, highlighting differences in quality between 2D and 3D calculations, with 2D calculations often proving more practical in terms of computational time and yielding satisfactory results.

Fread used dam break modelling to analyse the consequences of floods caused by earth embankment dam breaks due to meteorological conditions [15].

Moreover, Yudianto et al. [16] emphasised the significance of dam break analyses in assessing inundation risks resulting from severe meteorological conditions. These analyses differ from those typically undertaken for dam certification during construction or authorization procedures, where analysts have detailed information and ample time to prepare and conduct case studies and risk assessments. In the context of emergency calculations, production time is a critical factor, and initial and boundary conditions might not be fully available. Nevertheless, the analyses must be completed within the shortest possible timeframe and with only the available data to inform decisions on evacuation and other preparedness and response measures.

This study highlights the ability of this approach to provide timely and high-quality information on the development and consequences of rapid-onset events, proving to be a valuable asset for emergency response and risk management.

3.2. Analytical Methodology

As per the methodology outlined by Annunziato et al. [1], the data were prepared to account for the water reservoir level upstream of the dam at its maximum height, which corresponds to the height of the crest of the dam. As per the SRTM DEM, which was used to perform the computations [7], the crest height is 215 m at its centre, while according to the Google Earth DEM, the value is 205 m. However, both sources suggest that the dam edges lie at a higher level (approximately 229 m) than its centre (either 215 or 205 m), which is not possible, as the crest of the dam is flat. Therefore, given the uncertainty around the actual absolute height of the dam crest, four different water levels were taken into consideration, namely 205, 215, 225, and 230 m (Figure 5). It is worth mentioning that during the event, it is unknown whether the overfill discharge pipe (Figure 6) was operational or not, either due to its inability to contain the excess water or because it was obstructed and could not perform its intended function. This means that the initial overflow could have been characterised by an even higher water level than the crest height.

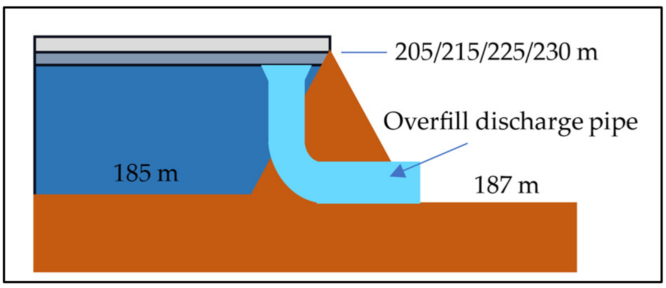

Figure 5. Dam geometry.

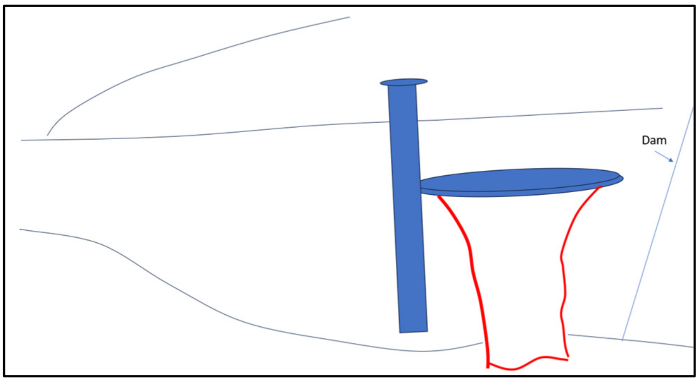

Figure 6. Drawing from image of Derna Dam overfill discharge pipe (image acquired from Erges) [17].

We should also note that the downstream Mansour Dam was not factored into the modelling, as it was reasonably assumed that it had already been destroyed or was immediately affected by the dam break flood. More details on this aspect are provided in Section 4.1.

3.3. Numerical Methods

In general, the analysis of a dam break through numerical modelling requires a significant amount of input data and output quantities. The applied methodology [1] aimed to establish a procedure that streamlines the preparation of the input deck and the derivation of the output quantities to enable a rapid analysis of a dam break event using the NAMIDANCE shallow-water model as the analytical tool [18,19]. This is crucial when, due to the urgency of understanding an ongoing or predicted event, a swift estimation of the potential impact is necessary. For the case of Derna, in the aftermath of the dam break event, very limited information was available to the international community to evaluate the consequences of the extensive flooding, while meteorological conditions did not allow for proper image acquisition and assessment.

NAMIDANCE has undergone validation through several benchmark problems and cross-code comparisons and has been applied to numerous tsunami events and modelling studies [19,20]. While NAMIDANCE has not been previously validated for dam break calculations, the tragic nature of this event presents an opportunity to assess the quality of the model for dam break simulations. The validation of the dam break scenario through the actual event is made possible by the availability of detailed satellite image analyses conducted by two independent expert teams from EU Copernicus EMS [21] and UNOSAT [22]. Furthermore, the JRC recently published a report that incorporates field reports and social media image analysis [10] and further enhances the quality of the validation exercise.

The calculations were performed using the Dam Break Platform [23], which allows the conditions to be set and subsequently performs the computations using NAMIDANCE. The DEM used for the Derna Dam calculations is the SRTM-30 m [7] resampled at 7.5 m. Each calculation was performed over a 24 h period to ensure that the dam reservoir was completely depleted of water and that the maximum flood extent was reached, even if, according to the calculations, this was reached in less than three hours. All processing was automated through the platform and is available for reference and consultation [23]. As the dynamics and extent of the dam break were unknown, an almost complete destruction of the dam was assumed in the modelling for the nominal case. Later on, this assumption was confirmed by the available post-event images, revealing extensive damage and significant sections destroyed (Figures 7 and 8).

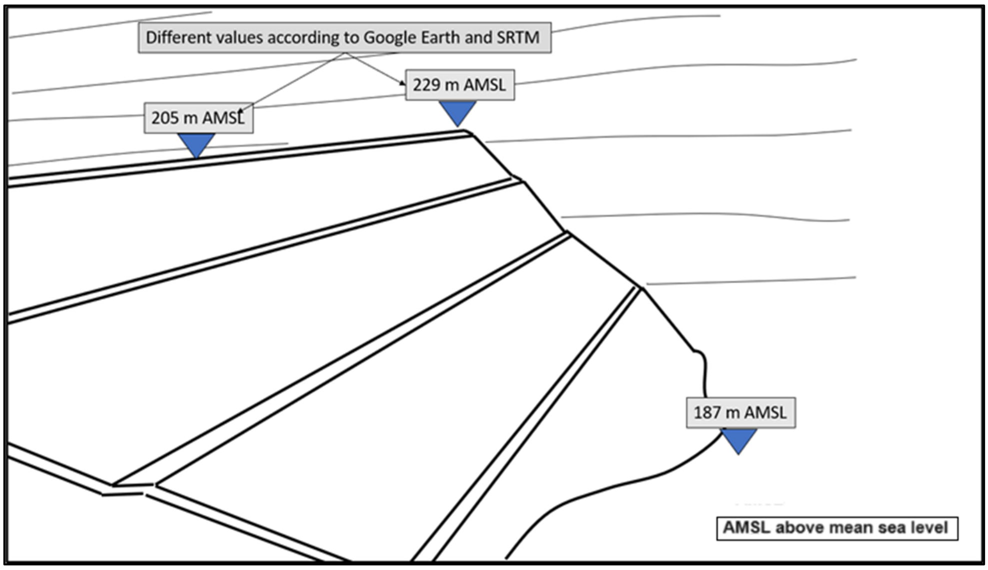

Figure 7. Drawing from image of the original form of the dam before the collapse (image acquired from DredgeWire) [24].

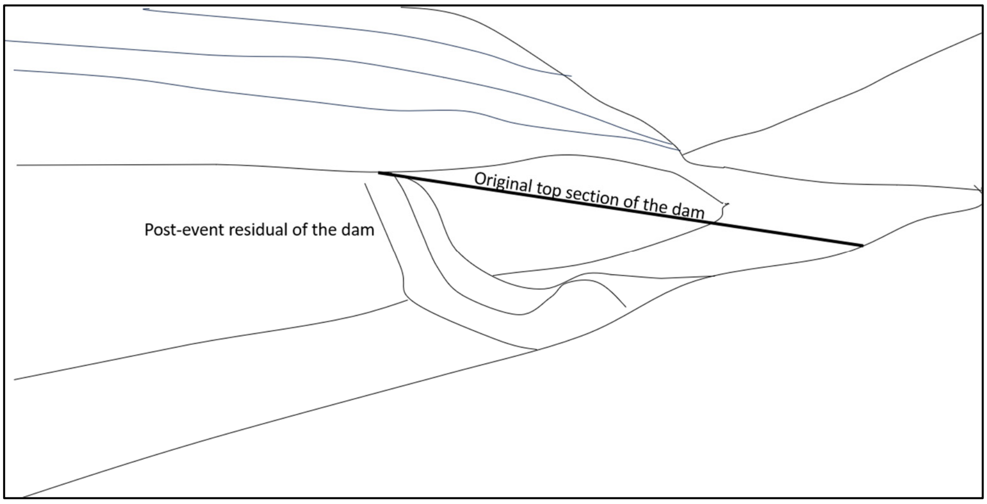

Figure 8. Drawing from image of the destroyed dam (image acquired from Eduvast) [25].

4. Derna Dam Break Scenario Modelling

4.1. Calculation of Nominal Case

The nominal case is performed considering a lake level height of 225 m above sea level, which is 10 m higher than the nominal elevation of the dam based on SRTM data. With these conditions, according to the scenario, the dam break would occur instantaneously, with a width of 260 m, which corresponds to 87% of the total crest width of 300 m. Subsequent sensitivity analyses, as discussed in the next section, showed that a width larger than 150 m does not substantially change the results because the narrow morphology of the upstream reservoirs limits the flow rate of the discharge. In the analysis, a Manning roughness coefficient of 0.015 $s/m^{1/3}$ was assumed to account for water flow resistance. The downstream river was assumed to be dry, in line with historical images from Google Earth. Nevertheless, the intense rainfall associated with the event could have caused an increase in the river's water level before the dam break, which will be the subject of a detailed analysis in the next sections.

The Mansour Dam was excluded from the analysis, as its break was assumed to be immediate. In fact, considering the initial modelled water flow rate of 49,720 m^3/s

resulting from the break of the upstream dam, the maximum capacity of the Mansour reservoir of 1.5 Mm^3 would have been reached in less than 1 min. This assumption would have been valid if the reservoir were completely dry, but given the heavy rains of those days, this may not have been the case; therefore, the timeframe could have been even shorter. Consequently, the arrival time of the flood in the city of Derna would have been delayed by only one minute or even less.

The bounding box of the analysis is defined by the coordinates (22.528468, 32.6370721) to (22.696805, 32.77986), with a grid comprising 2425 $\times$ 2057 cells. A time step of 0.6 s was selected for the stability of the Courant number. The calculations were performed using a Windows server equipped with an NVIDIA GeForce RTX 3060 GPU card, with a typical runtime of approximately one hour and 25 min for a 24 h problem duration and about 40 min to process the results.

The calculated water flow from the dam break can be observed in the figure below, which shows water propagation every 10 min. In fact, Figure 9 indicates that under these conditions (reservoir water height at 225 m, break size of 260 m, Manning roughness coefficient set at 0.015 $s/m^{1/3}$, and empty downstream river), Derna would have been reached by water in less than 30 min, causing significant flooding in a large portion of the city.

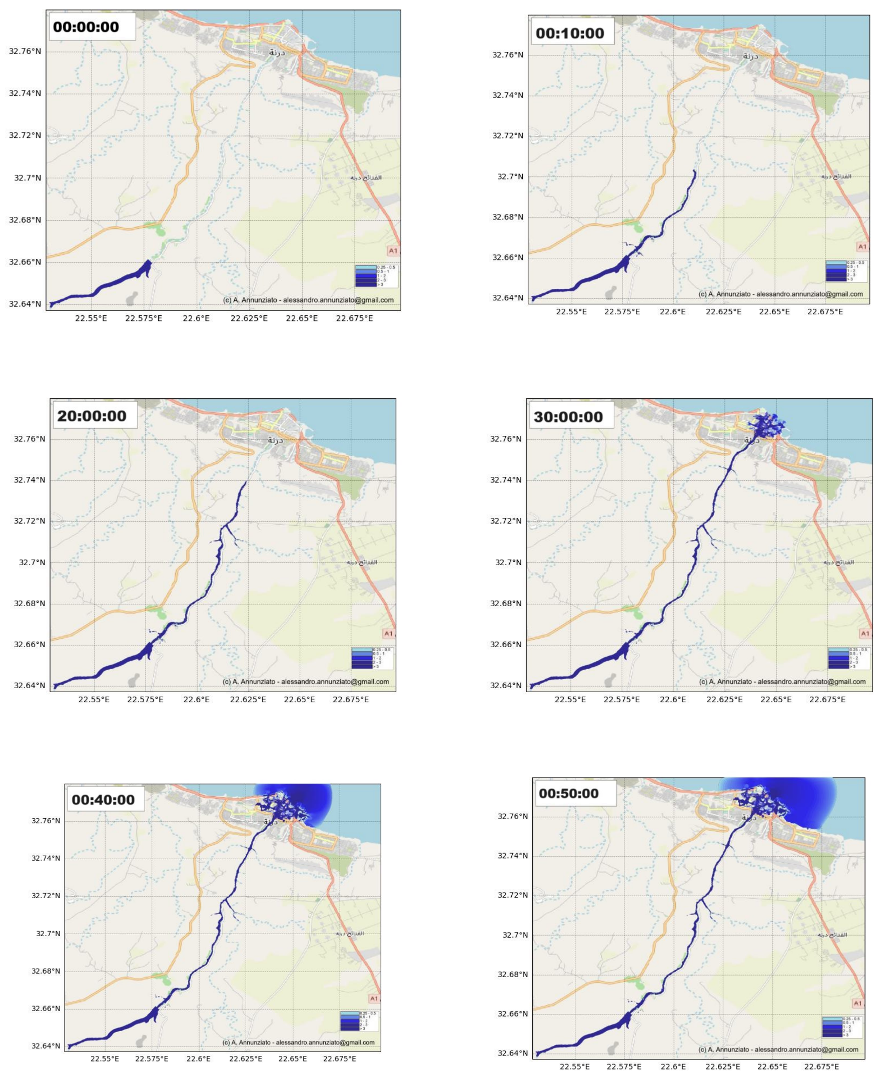

Figure 9. Calculated water propagation in the first 50 min following the Derna dam break, considering a reservoir water level of 225 m, a break size of 260 m, a Manning roughness coefficient set at 0.015 $s/m^{1/3}$, and an empty downstream river (basemap from OSM).

Table 2 presents the population affected by the event, categorised by water height. The combined population is approximately 111,000 based on the LandScan Global Populations 2014 model [26] and 71,000 according to the JRC Global Human Settlement Layer (GHSL) 2015 [27].

Table 2. Population affected by water height according to two population models (LandScan Global Populations 2014 and GHSL 2015).

Height Range (m)	LANDSCAN 2014	GHSL 2015
0.05–1.0	54,256	50,542
1.0–3.0	56,941	20,429
3.0–10	51	11
10–20	1	0
>20	0	0
Total	111,249	70,982

As already mentioned, the results discussed in this section can be accessed and consulted on the Dam Break Platform [23].

4.2. Sensitivity Analyses

Several details regarding the conditions at the time of the event remain unclear. Questions are still open regarding the rupture mode, including whether it was instantaneous or if it took some time to complete, as well as the size of the dam opening and the water levels in the reservoir before the break and in the downstream river.

It is assumed that prior to Storm Daniel, both the reservoir and the river were entirely empty and dry. Subsequently, as a result of the rainfall, the water level began to rise in the reservoir. It is unclear whether the water was released from the dam via the overfill discharge piping. If this was the case, the status and the level of the downstream river and that of the reservoir of the downstream dam would have been impacted, since they depend on the amount of water overflowing from the discharge pipe. However, the overfill pipe was probably inadequate or entirely ineffective in regulating water levels, ultimately causing the dam's destruction. However, the downstream river's level remains uncertain, ranging from completely dry to filled with water, depending on the amount of water overflowing from the overfill discharge pipe.

Given the uncertainties typical of these calculations, it was deemed necessary to conduct several sensitivity analyses to encompass the potential variations. Specifically, the following four parameters were considered: the initial water level of the upstream reservoir, the Manning roughness coefficient, the dam break width, and the level of the river downstream.

Regarding the reservoir's initial water level, we considered different hypotheses in addition to the nominal case described in the previous section, namely 205, 215, and 225 m above sea level. For the Manning roughness coefficient, we utilised the default value in the NAMIDANCE interface, 0.015 $s/m^{1/3}$, but we also examined lower and higher values (from 1/100 to 10 times) to verify the influence of this parameter on the results. In terms of the break size, while the nominal width of the dam is 300 m, our analysis of the SRTM indicates that the maximum break size could not exceed 260 m due to physical limitations imposed by the morphology of the valley itself, which, at its maximum height of 225 m, is approximately 260 m wide. As Figure 8 illustrates, at least 70–90% of the embankment appears to be missing as a result of the break, prompting the assumption of a nominal break width size of 260 m and a minimum size of 200 m, considering that in some sections, the break was not fully complete in height. For the level of the river downstream, three sets of arbitrary constant inlet flow values were imposed on the reservoir.

The calculation matrix is summarised in Table 3.

Table 3. Performed sensitivity analyses.

Lake Water Height (m)	Manning Roughness Coefficient (s/m$^{1/3}$)	Break Width (m)	Arbitrary Inlet Flows on the Reservoir Cells (m^2/s)
Lake water level (m)			
205	0.015	260	
215	"	"	
225	"	"	
230	"	"	
Manning Roughness Coefficient (s/m$^{1/3}$)			
225	0.00015	260	
"	0.0015	"	
"	0.015	"	
"	0.15	"	
Break width (m)			
225	0.015	30	
"	"	75	
"	"	100	
"	"	150	
"	"	200	
"	"	260	
Downstream River			
225	0.015	260	Dry river
"	"	"	0.0625
"	"	"	1.25
"	"	"	2.5

": This is the ditto mark, it indicates the same value as above.

4.2.1. Effect of the Lake Water Height

The initial water height of the lake was assumed to be between 205 and 230 m, considering the different SRTM data available for the area.

According to the calculation results shown in Table 4, as the water level rises in the upstream area, the initial peak flow also increases. For a reservoir water height of 225 m, the peak flow would reach a value of 49,720 m^3/s. Consequently, as illustrated in Figure 10, the arrival time would decrease from 83 to 20 min due to a significantly larger flow and depth in the river valley.

Table 4. Results of calculations with lake water height parameters.

	205 m	215 m	225 m	230 m
Discharged volume (million m^3)	4.3	20.14	48.2	61.7
Peak flow rate (m^3/s)	2493	27,357	49,720	65,003
Arrival time at Derna city entrance * (min)	83	26.0	21.0	20.0
Maximum flood wave height at the entrance of Derna * (m)	5.9	15.6	25.2	28.6

* Lat/Lon: 22.62784/32.74522.

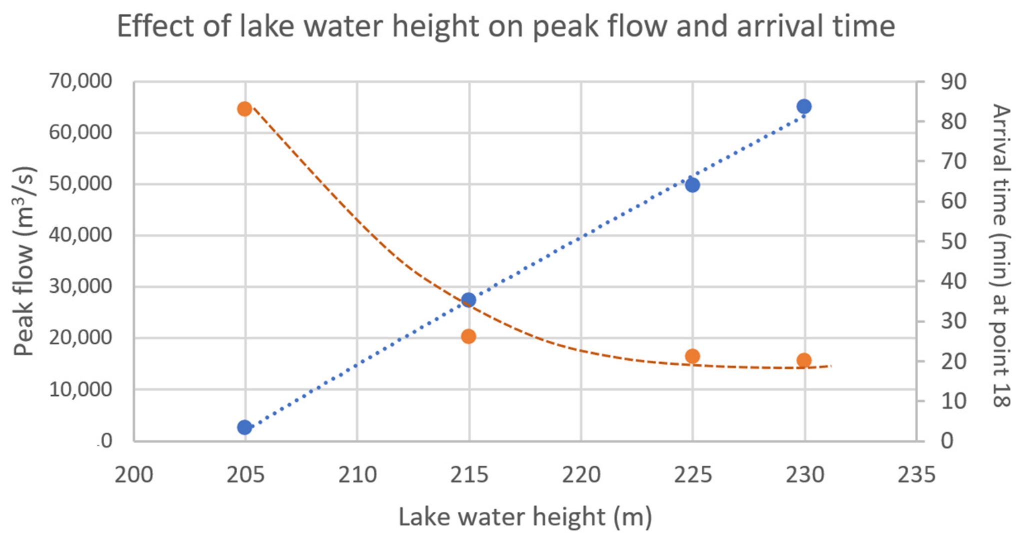

Figure 10. Effect of lake water height on peak flow (blue line) and arrival time (orange line) in Derna (22.62784/32.74522).

As per the model's results, the increase in the lake water level causes an increase of the initial peak flow, and as a result, the water level at the entrance of Derna increases notably from 5.2 to 28.6 m in the case of the highest lake water height (Figure 11). The resulting inundation extent in Derna would not change as much as the peak flow (Figure 12). Nevertheless, an increase in the inundation extent is noticeable with the increase in the lake elevation.

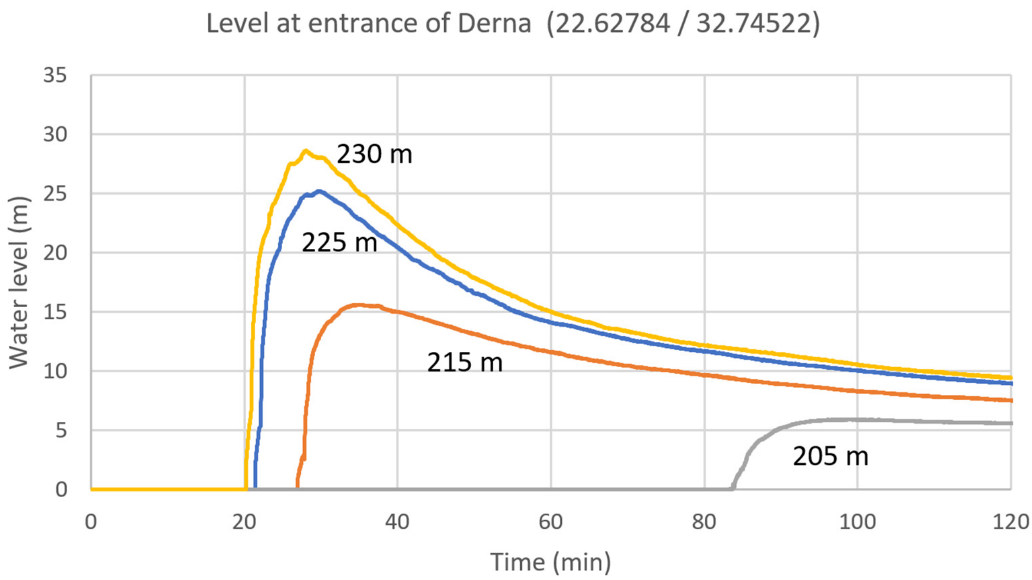

Figure 11. Flood water level at the entrance of Derna (22.62784/32.74522) with different lake water heights.

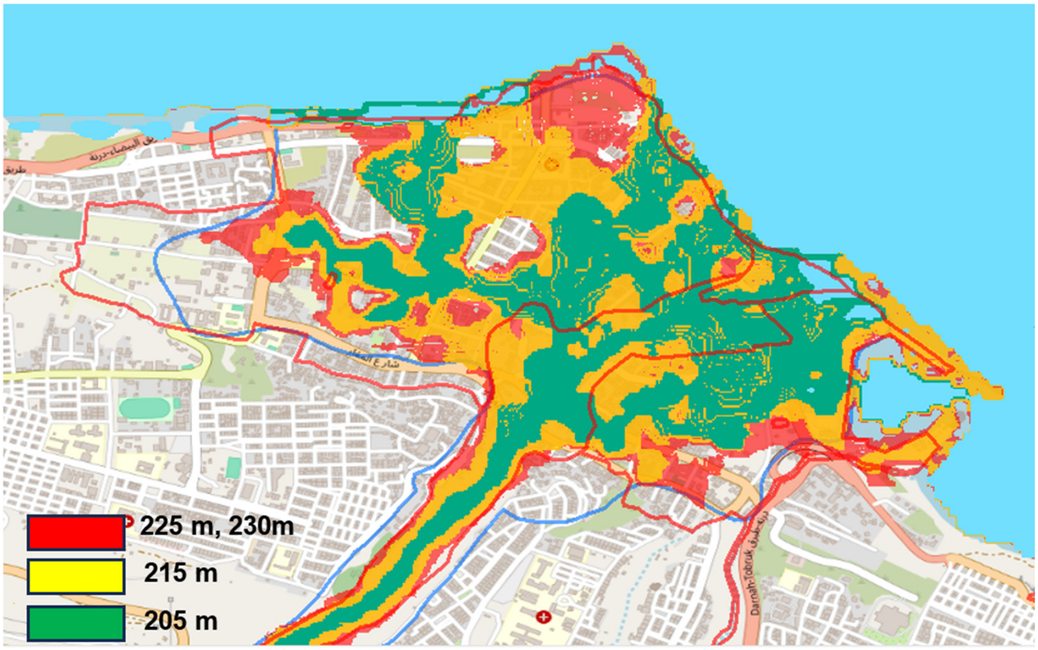

Figure 12. Effect of initial lake water height on the flood extent in Derna. The red line represents the flood extent assessed by Copernicus EMSR696 [21], and the blue line corresponds to UNOSAT FL20230912 as of 13 September 2023 [22] (basemap from OSM).

4.2.2. Impact of Manning Roughness Coefficient

All calculations involving different parameters for the Manning roughness coefficient were conducted using an initial water level of 225 m and a break width of 260 m.

As evident in Table 5, when the coefficient is increased from 0.0015 to 0.0015, then to 0.015 s/m$^{1/3}$, there are minimal changes in the peak flow, arrival time, and maximum flood wave height at the entrance of Derna, while a notable change is observed when the coefficient is increased by a factor of 10 to 0.15 s/m$^{1/3}$ (Figures 13–15).

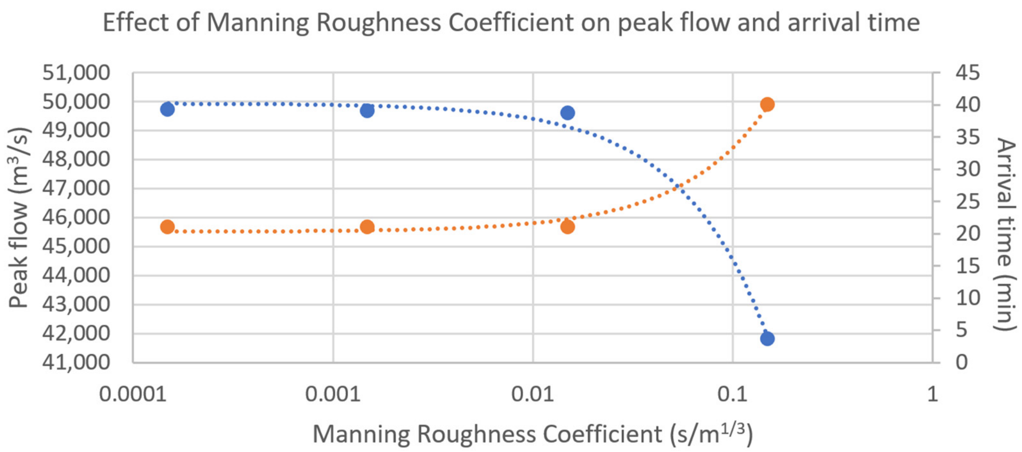

Figure 13. Effect of Manning roughness coefficient on the peak flow (blue line) and the arrival time (orange line) at the entrance of Derna (22.62784/32.74522).

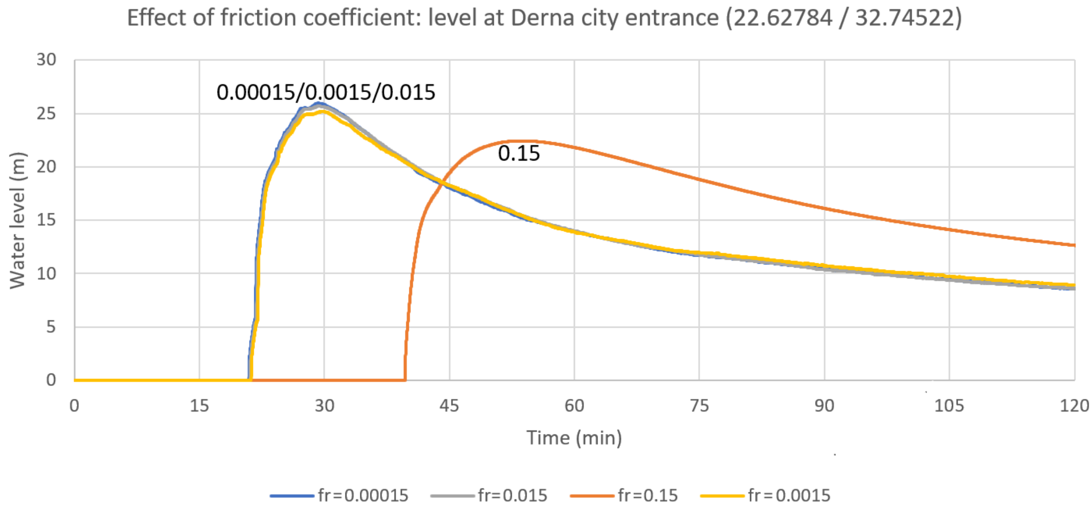

Figure 14. Flood wave height at the entrance of Derna (22.62784/32.74522) with different Manning roughness coefficients.

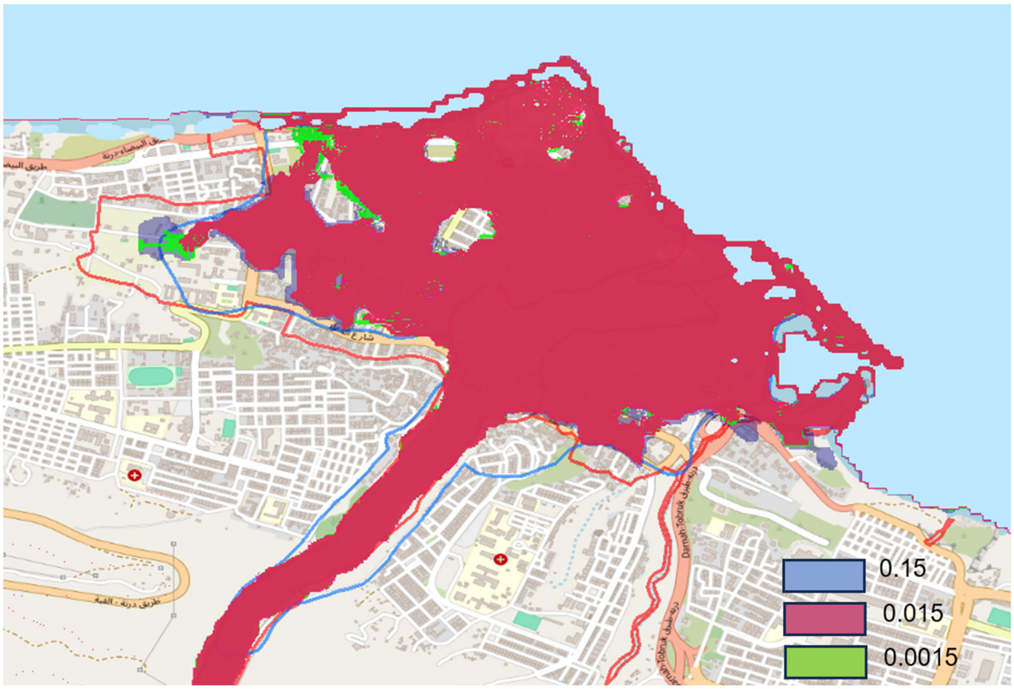

Figure 15. Effect of Manning roughness coefficient (s/m$^{1/3}$) on flooding in Derna. The red line represents the flood extent assessed by Copernicus EMSR696 [21], and the blue line corresponds to UNOSAT FL20230912 as of 13 September 2023 [22] (basemap from OSM).

Table 5. Results of calculations with Manning roughness coefficient parameters.

Manning roughness coefficient (s/m$^{1/3}$)	0.00015	0.0015	0.015	0.15
Discharged volume (million m^3)	49,887	49,852	49,720	41,175
Peak flow rate (m^3/s)	49.70	49.67	49.60	41.79
Arrival time (min)	21.0	21.0	21.0	40.0
Maximum flood wave height at the entrance of Derna * (m)	25.3	25.2	25.2	22.3

* Lat/Lon: 22.62784/32.74522.

4.2.3. Effect of Break Width

This section focuses on the impact of the break width, considering that all calculations were performed with an initial lake water height of 225 m and a Manning roughness coefficient of 0.015 s/m$^{1/3}$. The results are shown in Table 6.

Table 6. Results of calculations with different dam break width parameters.

	30 m	**75 m**	**100 m**	**150 m**	**200 m**	**260 m**
Discharged volume (million m^3)	48.2	48.2	48.2	48.2	48.2	48.2
Peak flow rate (m^3/s)	13,326	29,894	36,123	48,788	50,279	49,720
Arrival time (min)	31	23	22	21	21	21
Maximum flood wave height at the entrance of Derna * (m)	16.7	22	23.5	25	25	25.2

* Lat/Lon: 22.62784/32.74522.

It is notable that by increasing the parameter of the break width up to 200 m, the peak flow increases and the arrival time decreases (see Figure 16). Beyond this value, the changes become marginal. This is due to the morphology of the upstream reservoir, which, in some sections, is smaller than 200 m.

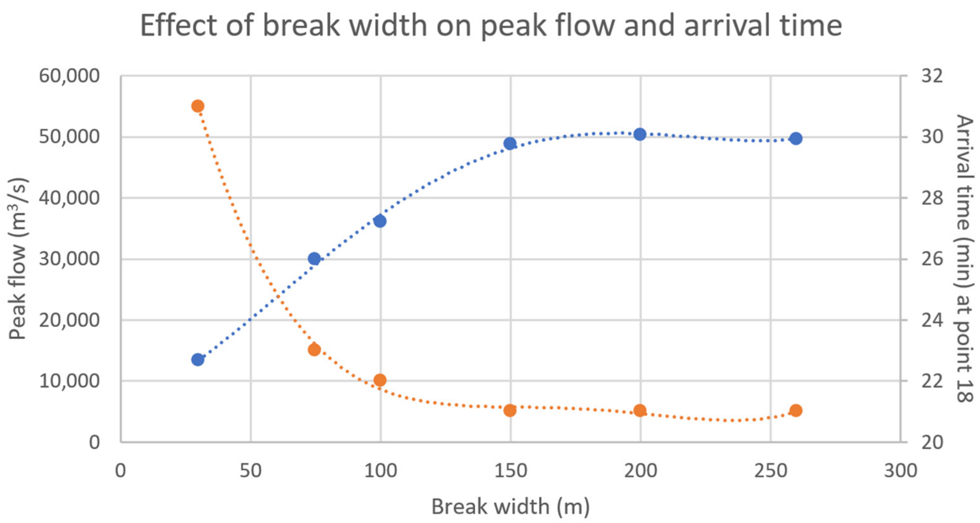

Figure 16. Effect of break width on the peak flow (blue line) and the arrival time (orange line) at the entrance of Derna (22.62784/32.74522).

4.2.4. Presence of River Flow Downstream of the Break

A sophisticated technique was employed to perform river flow calculations, as it is challenging to accurately consider the conditions during or just before an overflow event. The overflow was simulated by imposing a constant inlet flow in the upstream reservoir. As the overflow commenced, the flow began to spread across the river floodplain, with the depth of the river varying along its course, influenced by the outlet flow rate and the slope of the river in each location. In the literature, we found a similar method to take into account the initial river condition [28].

The overspilling was considered to last for 7 h, which is the time required for the water to reach the lower dam according to the calculation. The break could have occurred at any time during this period, although it typically occurs much sooner (see Figure 17). According to Froelich [29], all cases examined in his analysis displayed a break formation time of less than 1 h, with the sole exception of 8.5 h for the Oros Dam in Brazil.

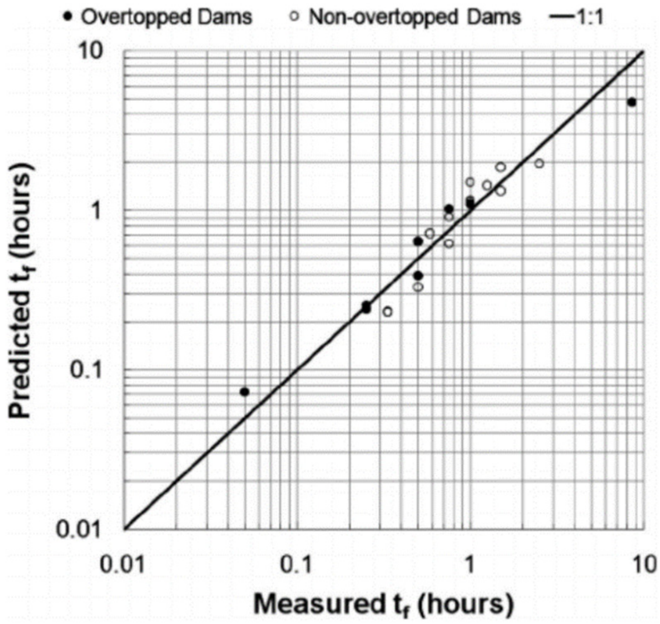

Figure 17. Measured and predicted break formation times, Froelich [29].

According to Froelich, the formation time for a potential dam break can be calculated using the following experimental formula:

$$T_f = 63.2\sqrt{\frac{V_w}{gH_b^2}}$$

where V_w represents the volume of water, and H_b represents the height of the dam. When applying this formula with the parameters specific to our case, that is, V_w = 18 Mm^3 and H_b = 75 m, the resulting time is calculated to be 1.1 h. This calculated time represents the expected duration required for a break to form based on the given water volume and dam height. However, the actual time of seven hours significantly exceeds this expected breaking time.

During the considered 7 h overspilling, three sets of arbitrary constant inlet flow values were imposed on the reservoir. When overtopping occurs, the water is discharged into the river plain, causing it to progressively fill up. The assumption is that the break would occur after the 7 h overspilling. The calculated water level along the river at the end of the 7 h was assumed as the initial condition for the river water level in the dam break calculation.

According to this scenario, once the break occurs, the travel time is significantly reduced compared to the dry case, as the wave velocity is higher due to the overall water height calculated as the sum of the river depth and the wave on top. Therefore, the velocity of the wave (v) is higher, as it is approximately v = $(g\ D)^{1/2}$, where D represents the overall water height and g is the gravity constant. By increasing the water level in the river, the arrival time decreases from 21 to 16 min, as shown in Figure 18.

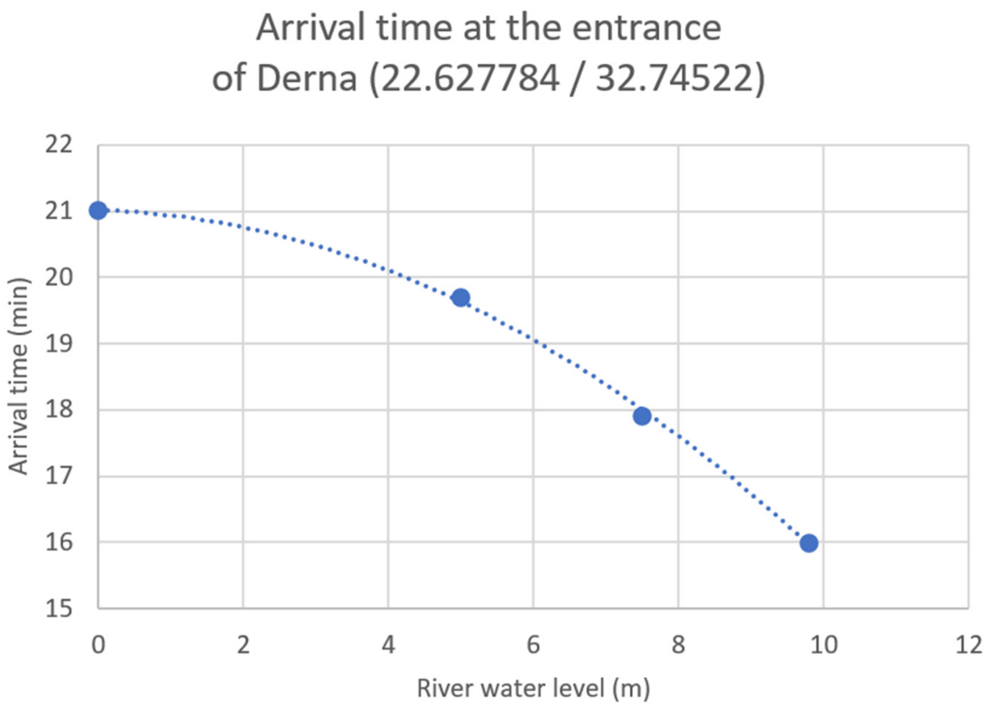

Figure 18. Arrival time as a function of initial water level in the river.

The modelled maximum water level at the entrance of Derna increases with the rise in the initial water level in the river, although not significantly, as shown in Figure 19.

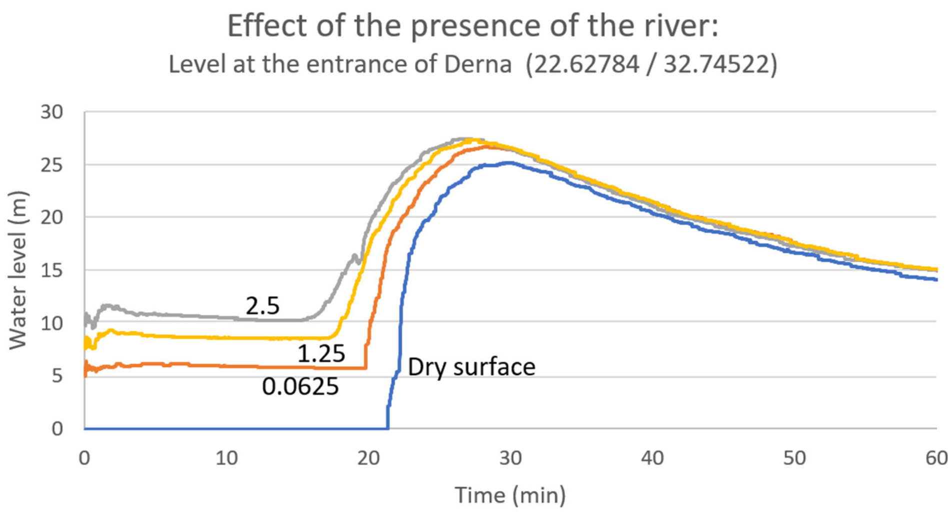

Figure 19. Effect of the presence of the river downstream of the dam when imposing 0.0625, 1.25, or 2.5 m^2/s as flux in each cell of the lake reservoir.

Therefore, the rising river level has a direct impact on the extent of downstream inundation, resulting in a more extensive area being affected, as illustrated in Figure 20.

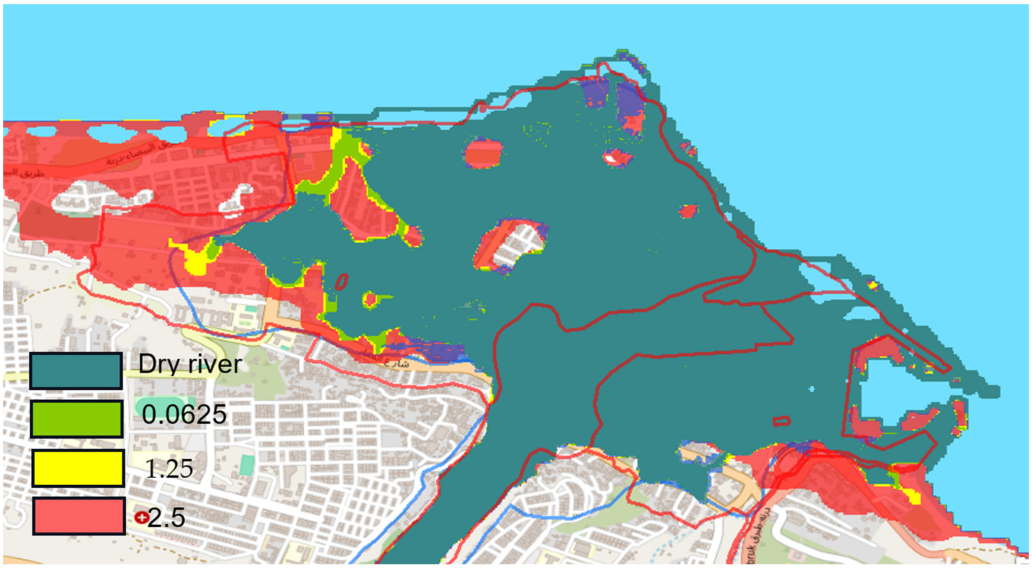

Figure 20. Effect of river flow on Derna inundation. The red line represents the flood extent assessed by Copernicus EMSR696 [21], and the blue line corresponds to UNOSAT FL20230912 as of 13 September 2023 [22] (basemap from OSM).

5. Model Validation

To validate the modelling results, we used a variety of available data sources, such as local reporting, post-event satellite mapping from Copernicus Emergency Management Service—Rapid Mapping, and information from social media. The integration of these diverse data sets enabled temporal and spatial validation.

5.1. Temporal Validation

As per the dam break scenario with the maximum reservoir water level height (230 m) and maximum break width (260 m), the water flow would take approximately 27 min to reach the nearest urban area of Derna (see Figure 9). It would reach the sea in around 40 min, and the maximum flood extent in Derna would be reached within 60 min.

The calculated flood travel time is illustrated in Figure 21, which indicates the arrival time across various time intervals. The water would arrive at the nearest urban area of Derna in approximately 25 min, and within another 10 min, most of the inundation would occur.

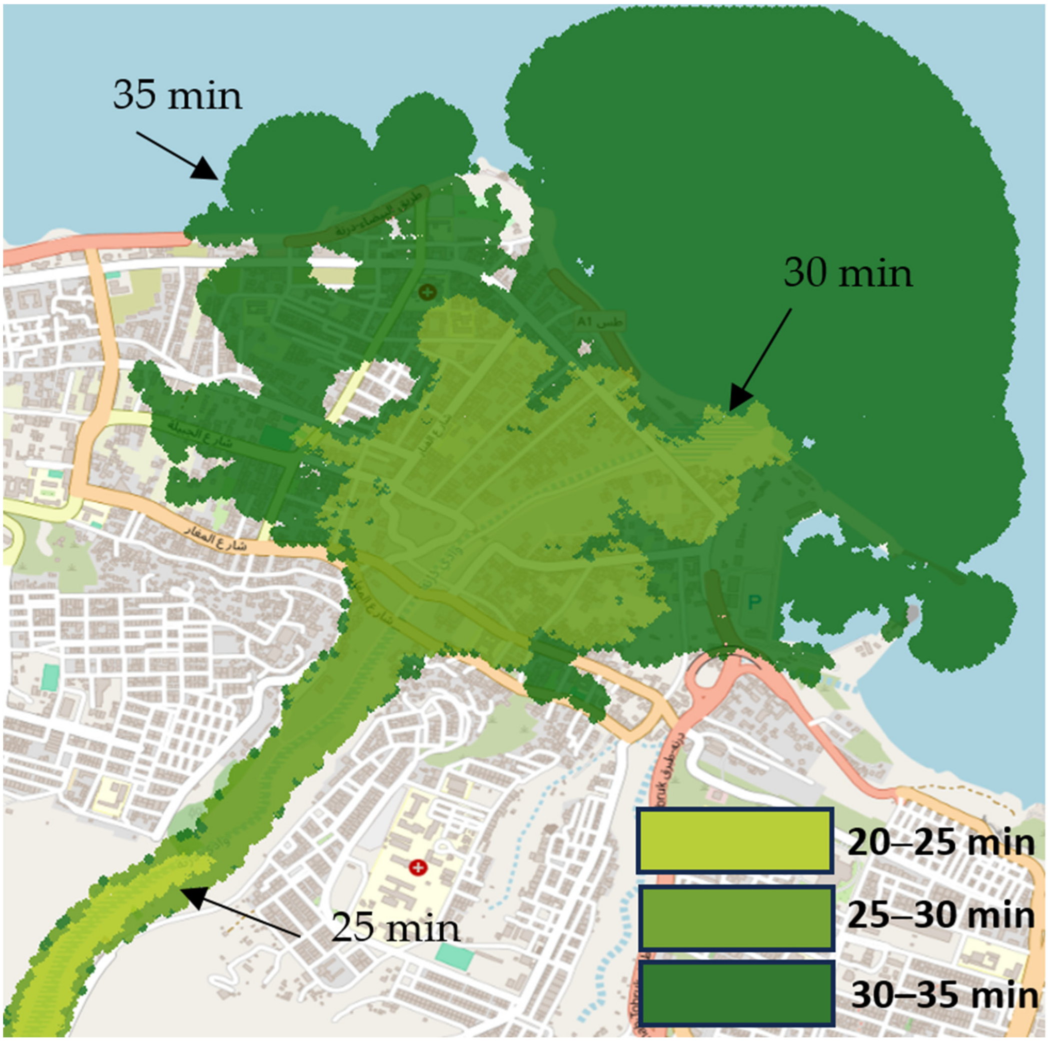

Figure 21. Calculated flood travel time (basemap from OSM).

These timeframes align closely with first-hand testimonies collected remotely by international experts, referring an approximate arrival time of around 30 min for the first arrival of the flow in the city (Figure 22).

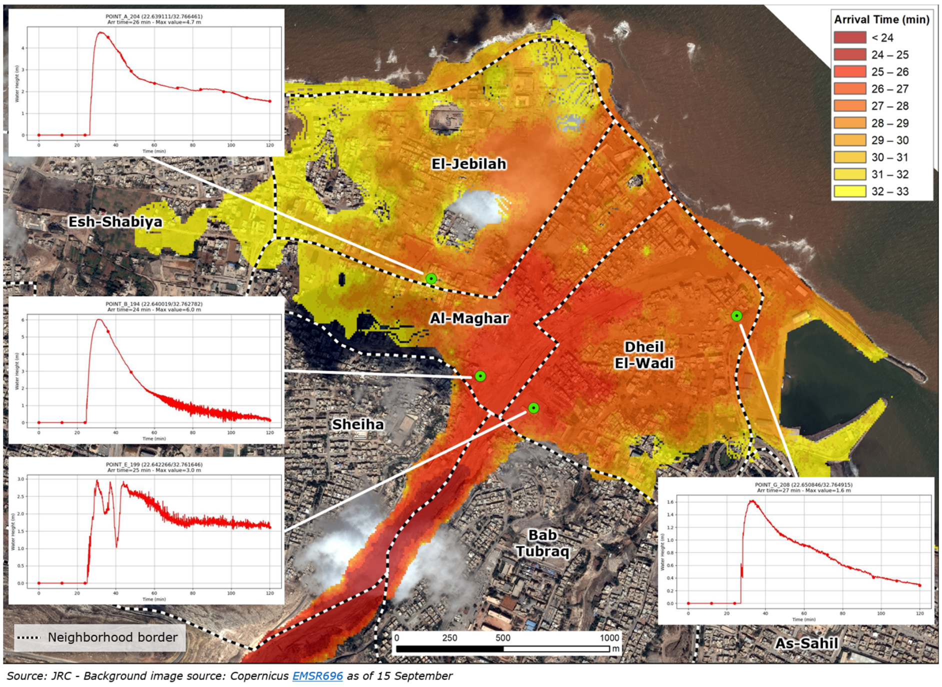

Figure 22. Flood arrival times in Derna (JRC and basemap from Copernicus).

Another aspect of the temporal validation process involves measuring the rate at which the flow depth increases over time. In this regard, a social media image collection and visual interpretation were conducted to determine the water depth in specific locations. For instance, data from security cameras in the Al-Maghar neighbourhood, which experienced the most significant flood extent and impact, indicated a water level rise of approximately two metres in less than one minute [30]. When comparing this observation with the charts in Figure 23, representing the simulation outcomes from the Al-Maghar neighbourhood, the order of magnitude is consistent.

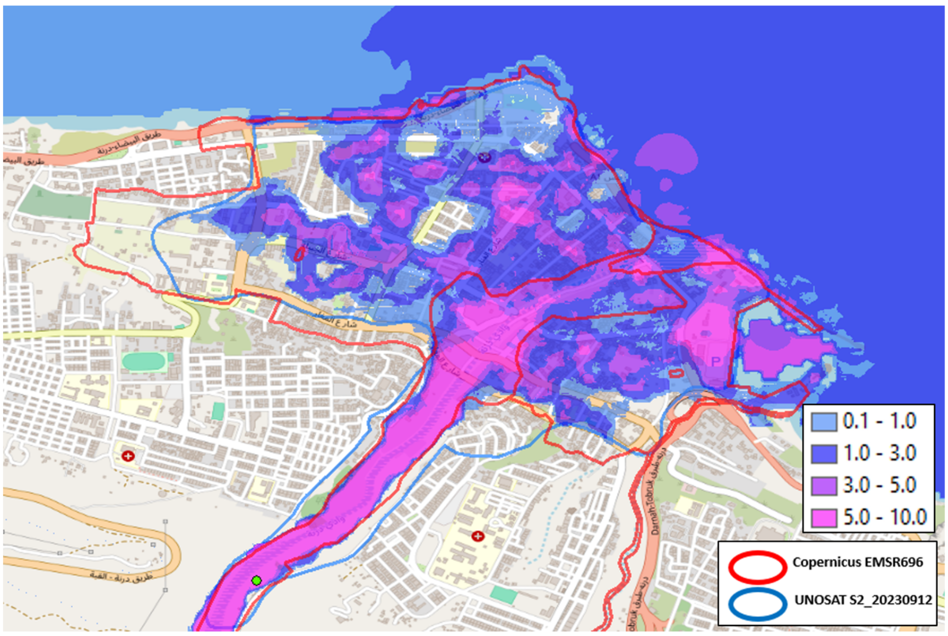

Figure 23. Maximum flow depth for the nominal case in the Al-Maghar neighbourhood. The computed data are compared with the flood extents identified by UNOSAT (blue line) [22] and Copernicus EMS (red line) [21] (basemap from OSM).

5.2. Spatial Validation

Figure 23 shows the modelled maximum flood extent, revealing that a substantial part of the Derna's city centre would have experienced flow depths exceeding 5 m. Moreover, the sea level in front of Derna would have experienced a rise, with depths ranging from 1 to 3 m. In particular, in the eastern coastal area, the water level would have increased by up to 1.15 m, suggesting potential coastal inundation in a significant portion of the eastern city. During the validation of the scenario with the actual event, the comparison of flood extents with Copernicus EMS [21] and UNOSAT [22] appeared to be largely accurate. However, some discrepancies were observed, particularly in western Derna, where some areas appeared unaffected in the calculation but were flooded according to satellite assessments.

These discrepancies are attributed to small variations in elevation in the SRTM digital elevation model [7], which would have obstructed water entry and flows into these areas (refer to the lower portion of Figure 24). It is unclear whether these are artefacts of the SRTM or actual elevated areas without local investigation. Moreover, the designation of these locations as 'flooded' or 'affected' by UNOSAT or Copernicus experts may indicate wet areas resulting from heavy precipitation rather than flooding due to the dam break. It is also important to note that the SRTM does not consider the presence of buildings, which can significantly alter water flow by creating channelling and higher-velocity paths.

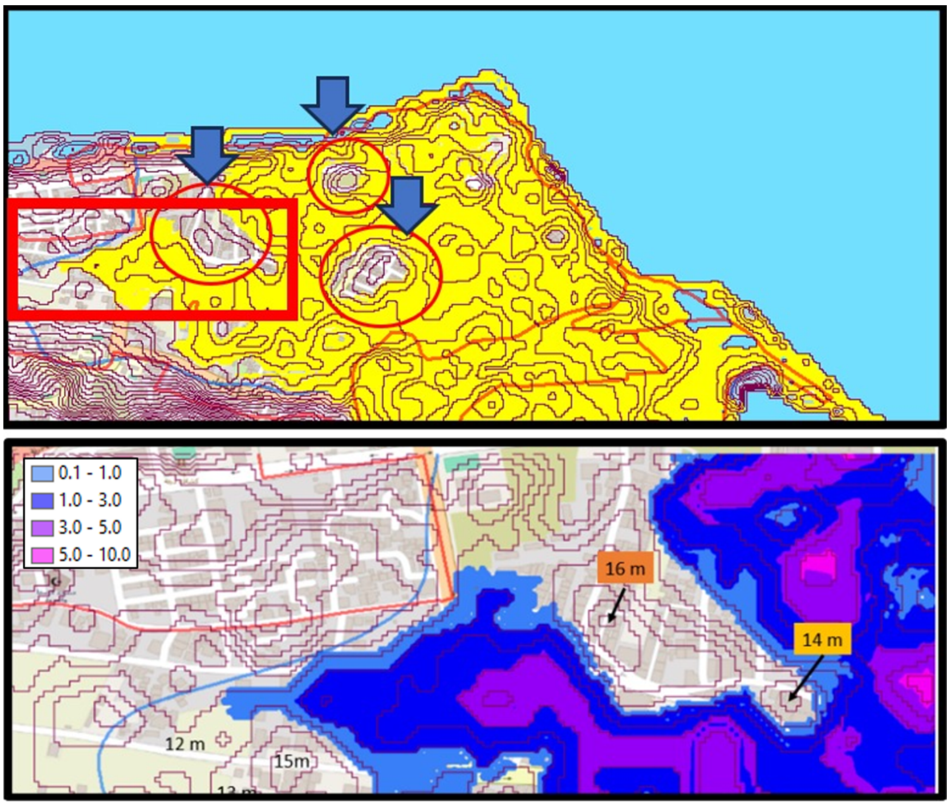

Figure 24. Top figure: SRTM contour [7] with flow depth greater than 0 in yellow; the blue arrows indicate elevated areas. Bottom figure: SRTM contour [7] with the detailed maximum flow depth (basemap from OSM).

The overall flooded area is detailed in Table 7. Both UNOSAT and Copernicus analyses estimated the overall area to be between 3.1 and 3.3 km^2, while the scenario indicates a slightly lower value of approximately 2.7 km^2.

Table 7. Inundated surface.

Mode	Surface (km^2)
UNOSAT	3.1
Copernicus	3.3
WL = 225 BW = 260	2.7

5.3. Flow Depth Validation

Ideally, field teams measuring flood heights relative to common reference points are deployed as early as possible to assess flow depths following sudden-onset and extensive flood events, as in the case of tsunami events. However, in this case, the assessment was conducted remotely by the international community.

To evaluate the accuracy of the flow depth in the model, a number of identifiable landmarks were selected and used to estimate the flow depth by visually analysing post-event images from social media referred to these points. Artificial intelligence techniques were utilised to extract flood images from social media, and text mining was applied to locate images containing information about water depth.

The visually interpreted water depth values were compared to the model-derived ones, revealing that the flood depth was generally underestimated. This discrepancy may be attributed to the same factors influencing the previously mentioned underestimation of flood extent, namely the height variations in the STRM [7] (refer to Figure 23). Additionally, it is important to note that the model does not account for the splash effects that can occur at the forefront of the flood wave. These splash effects might leave wet traces on building facades at higher levels with respect to the actual flood depth.

The results of the visual interpretation of the water height from the analysis of social media images compared to the modelled flood depths at selected locations are presented in Figures 25 and 26 and in Table 8. A list of image sources for selected locations can be found in Appendix A. The comparison of the visual interpretation of the images with the modelling results revealed an average underestimation of modelled flood depth of approximately 13% for the 230 m lake water level case and 17% with the 225 m case.

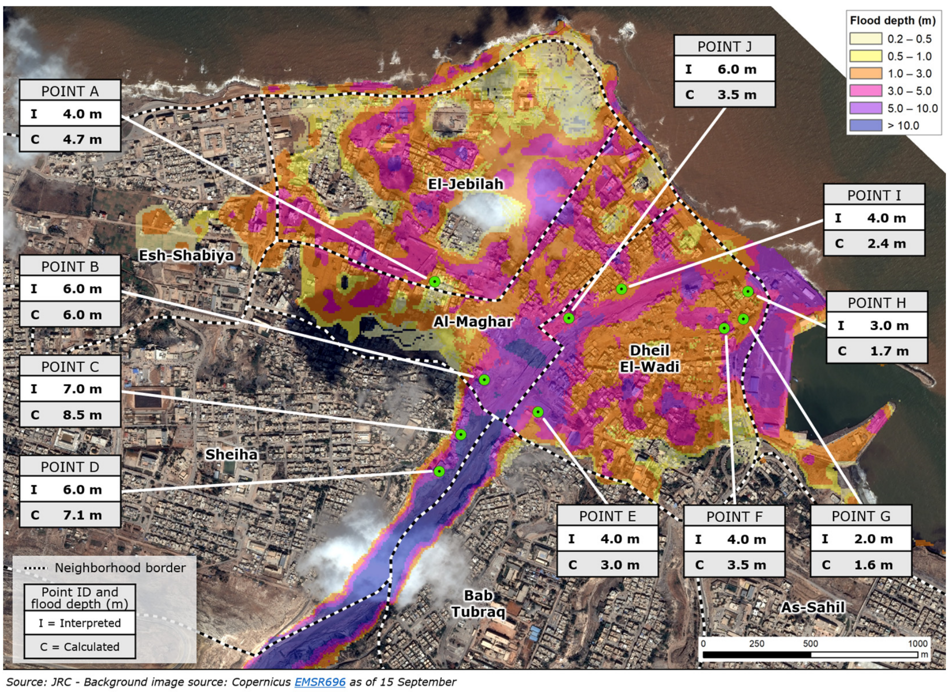

Figure 25. Comparison of the flood depth from modelling and from visual interpretation of images at selected locations (JRC and basemap from Copernicus).

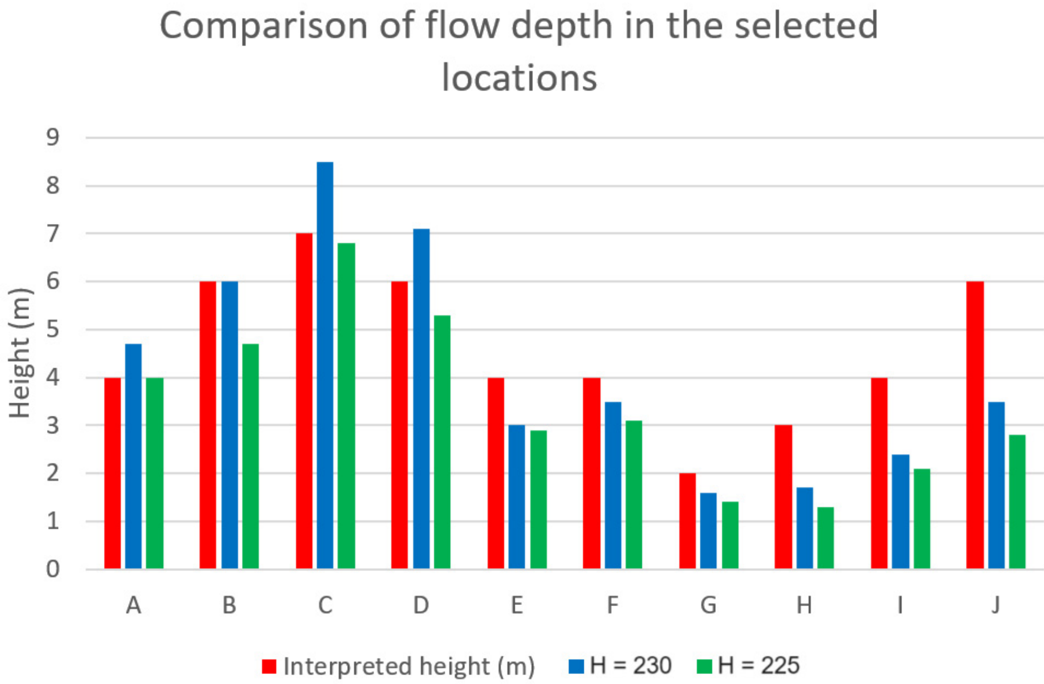

Figure 26. Comparison between interpreted and modelled flood depths at selected locations. Red bars: visual interpretation from social media; blue bars: model results with an assumed water height in the reservoir of 230 m; green bars: model results with an assumed water height in the reservoir of 225 m.

Table 8. List of selected locations and comparison of the flood depth values.

ID	Latitude	Longitude	Interpreted Flood Depth (m)	Calculated Height (230 m Case) (m)	Calculated Height (225 m Case) (m)	Delta for 230 m Case (%)	Delta for 225 m Case (%)
A	22.639111	32.766461	4.0	4.7	4	−18	15
B	22.640019	32.762782	6.0	6.0	4.7	0	22
C	22.639033	32.760849	7.0	8.5	6.8	−21	20
D	22.638136	32.759563	6.0	7.1	5.3	−18	25
E	22.642266	32.761646	4.0	3	2.9	25	3
F	22.65005	32.764593	4.0	3.5	3.1	13	11
G	22.650846	32.764915	2.0	1.6	1.4	20	13
H	22.651043	32.765885	3.0	1.7	1.3	43	24
I	22.645749	32.765969	4.0	2.4	2.1	40	13
J	22.643552	32.764949	6.0	3.5	2.8	42	20
		Average Difference (%)				13	17

6. Main Findings

The results of the validation exercise of the Derna dam break scenario conducted by integrating satellite mapping, media and social media images, and reports collected remotely from local testimonies are summarised in this section.

6.1. Temporal Assessment

Although the exact time of the dam break remains unknown, reports collected remotely from local testimonies suggest an approximate arrival time in Derna of 30 min. Therefore, the modelled arrival time of 27 min can be regarded as a highly accurate estimation.

The rate of flood height increase was assessed using data from security cameras [31] at key observation points, including the Al-Maghar neighbourhood, the Al Sahaba Mosque, and other easily identifiable landmarks. In the most heavily affected areas, such as Al-

Maghar and the Mosque, the observed rate of increase was approximately two metres per minute. This observed value corresponds with the modelled increase in flow depth extracted from the same observation points, confirming the consistency of the model's estimations.

6.2. Spatial Assessment

A comparison of flood extent data from Copernicus EMS [21] and UNOSAT [22] suggests that the spatial extent of the flood is well represented by the model's results. The modelled flood extent in Derna is approximately 57 hectares smaller when compared to post-event satellite mapping and assessments. This discrepancy is deemed acceptable, as the model does not account for factors such as rainfall contribution and resulting water accumulation in the smaller downstream dam. Moreover, the model only considers areas as flooded when the water depth exceeds 10 cm.

6.3. Flood Depth Assessment

The comparison between visual interpretation of social media information extracted through artificial intelligence with the modelled flood depth revealed an average underestimation of approximately 13% in the 230 m lake water level case and 17% in the 225 m case, confirming substantial consistency.

7. Conclusions

This study reveals that the flood arrival time in the city of Derna would have been between 15 and 30 min, making it extremely challenging to provide advance warning to the population, even if an active early warning system had been in place. Unfortunately, this was not the case, as an automatic alert system was not present at the time of the event. This underscores the importance of emergency preparedness measures in dam safety protocols.

Upon comparing the estimated inundation extent across different scenarios with the delineation by UNOSAT and Copernicus satellite products, it was found that the majority of the flooded area was correctly identified by the model, accounting for approximately 82 to 84% of the total actual flood extent. In only one calculation, characterised by a very high initial river flow, the inundation exceeded the delineation of the flooded area derived from satellite imagery. The comparison of the maximum water depth indicates that the difference between the computed and estimated height was less than 20%. This analysis demonstrates the added value of the combined use of high-resolution satellite images and social media information processing to determine a detailed flood extent and water height for the event.

This approach allowed us to address some of the significant uncertainties in the initial conditions of the Derna dam break event, including a plausible water height of the reservoir of between 225 and 230 m, indicating that the dam break probably occurred with the reservoir at its full capacity. The validation exercise conducted using satellite and social media-derived images also confirmed the accuracy of the temporally and spatially modelled flood.

Overall, the validation exercise demonstrated the feasibility and substantial reliability of a rapid assessment of the dam break dynamic through the selected modelling approach, despite the lack of precise local measurements. Acquiring detailed topography up to 1 m resolution, such as through drone flights equipped with LiDAR instrumentation, would allow for a more accurate assessment. In the case of the Casamicciola landslide in Ischia, Italy, Copernicus drone flights obtained a post-event digital terrain model with 5 cm resolution within two days [1].

The low volume of the Mansour Dam downstream of the Derna Dam should not have had a significant influence on the dynamic of the inundation in the city of Derna. While for other cases of cascading dam collapses, with reservoirs of similar dimensions, specialised techniques (e.g., accounting for geometry changes during the calculation) may be required, for this particular scenario, the downstream dam's reservoir volume was likely not a major factor in the flooding.

In conclusion, the rapid modelling of dam break events and combined analysis of multiple data types have proven suitable for promptly assessing the expected dynamic of the event, as well as reconstructing the unknown initial conditions before the break. Incorporating sensitivity analyses provides an estimate of the uncertainties associated with the deduced values of the unknown parameters and their relative importance in the analysis.

Author Contributions: Conceptualization, A.A., M.S. and C.P.; literature search, A.A., M.S. and C.P.; methodology, A.A., M.S. and C.P.; study design, A.A., M.S. and C.P.; data collection, A.A., M.S., C.P. and V.L.; data processing, A.A., M.S., C.P., A.G. and M.T.; data analysis, A.A., M.S., C.P. and V.L.; data interpretation, A.A., M.S. and C.P.; writing—original draft preparation, A.A., M.S., C.P. and L.d.G.; writing—review and editing, A.A., M.S., C.P. and L.d.G. All authors have read and agreed to the published version of the manuscript.

Funding: This research received no external funding.

Data Availability Statement: The calculations were performed using the Dam Break Platform. Results are available for reference and consultation at https://github.com/annunal/DamBreak/tree/main/DBP.

Acknowledgments: The authors acknowledge Andrey Zaytsev for his efforts in developing the numerical structure of NAMI DANCE and Bora Yalciner for his outstanding success in developing a GPU version of NAMI DANCE.

Conflicts of Interest: Authors Chiara Proietti and Andrea Gerhardinger were employed by the company FINCONS SPA. And Author Ludovica de Girolamo was employed by the company Seidor Italy SRL. The remaining authors declare that the research was conducted in the absence of any commercial or financial relationships that could be construed as a potential conflict of interest.

Appendix A

Table A1. List of image sources for selected locations.

ID	Image/Location Source	Latitude	Longitude	Interpreted Flood Height (m)
A	Source: X/@YeniSafakArabic	22.639111	32.766461	4.0
B	Source: El Pais	22.640019	32.762782	6.0
C	Source: X/@Alhamdhulillaah	22.639033	32.760849	7.0
D	Source: X/@AhmedMussa218	22.638136	32.759563	6.0
E	Source: X@ @lole06554	22.642266	32.761646	4.0
F	Source: Al Jazeera/Jamal Alkomaty/AP Photo	22.65005	32.764593	4.0
G	source: X/@magazine_wafaa	22.650846	32.764915	2.0
H	Source: Jamal Alkomaty/AP	22.651043	32.765885	3.0
I	Source: Al Jazeera/Jamal Alkomaty/AP Photo	22.645749	32.765969	4.0
J	Source: X/@WorldTimesWT	22.643552	32.764949	6.0

References

1. Annunziato, A.; Guney Dogan, G.; Yalciner, A.C. Modeling Dam Break Events Using Shallow Water Model. *Eng* **2023**, *4*, 1851–1870. [CrossRef]
2. World Meteorological Organization Report. Provisional State of the Global Climate 2023. Report. 2023. Available online: https://wmo.int/sites/default/files/2023-11/WMO%20Provisional%20State%20of%20the%20Global%20Climate%202023.pdf (accessed on 20 May 2024).
3. International Organization for Migration. Resilience, Recovery & Reconstruction Plan, Storm Daniel. Report. 2023. Available online: https://reliefweb.int/report/libya/iom-libya-resilience-recovery-reconstruction-plan-storm-daniel-september-2023-september-2024 (accessed on 20 May 2024).
4. ECHO Daily Map of 13 September 2023. Available online: https://erccportal.jrc.ec.europa.eu/ECHO-Products/Maps#/maps/4636 (accessed on 20 May 2024).
5. Pielke, R. Trends in Flooding in Africa. Available online: https://rogerpielkejr.substack.com/p/trends-in-flooding-in-africa (accessed on 20 May 2024).
6. Technical Data on Derna and Mansour Dams on Hidrotehnika Company Website. Available online: https://www.hidrotehnika.rs/en/libya/wadi-derna/ (accessed on 20 May 2024).
7. SRTM Topography Database (NASA) via Watkins, D. 30-Meter SRTM Tile Downloader Method. Available online: https://dwtkns.com/srtm30m/) (accessed on 20 May 2024).
8. Abdalla, M. Mathematical Model of Dam Break: Applied Study of Derna Dam. *MEJ—Mansoura Eng. J.* **2002**, *27*, 46–59. [CrossRef]
9. Ashoor, A.A.R. Estimation of the surface runoff depth of Wadi Derna Basin by integrating the geographic information systems and Soil Conservation Service (SCS-CN) model. *J. Pure Appl. Sci.* **2023**, *21*, 90–100. [CrossRef]
10. Santini, M.; Proietti, C.; Gerhardinger, A.; Tucci, M.; Barantiev, D.; Giustolisi, L.; Lorini, V. *Validation Analysis of the Dam Breach Calculations for Derna Dam, Libya*; JRC136254; Publications Office of the European Union: Luxembourg, 2023; under review.
11. Imran, J.; Nemnem, A.; Tanim, A.; Khan, S.; Nahian, A.; Goharian, E. Rising Waters, Falling Dams: Deciphering the Derna Flood Disaster. *Nat. Portf.* **2024**. *preprint version*. [CrossRef]
12. Groenewege, R. Rapid simulation and assessment of the Derna (Libya) dam failures. Conference Paper. 2024. Available online: https://www.researchgate.net/publication/378961823_Rapid_simulation_and_assessment_of_the_Derna_Libya_dam_failures (accessed on 20 May 2024).
13. Prida, A. Dam Break Simulation in Derna (Libya) Using HydroMT_SFINCS. Presented at Delft Software Days, November 2023. Available online: https://softwaredays.deltares.nl/-/dsd-int-2023-slides-dam-break-simulation-in-derna-libya-using-hydromt_sfincs?startDate=06-09-2023 (accessed on 20 May 2024).
14. Akgun, C.; Nas, S.S.; Uslu, A. 2D and 3D Numerical Simulation of Dam-Break Flooding: A Case Study of the Tuzluca Dam, Turkey. *Water* **2023**, *15*, 3622. [CrossRef]
15. Fread, D.L. Dam-Breach Floods. In *Hydrology of Disasters*; Singh, V.P., Ed.; Water Science and Technology Library; Springer: Dordrecht, The Netherlands, 1996; Volume 24. [CrossRef]
16. Yudianto, D.; Ginting, B.M.; Sanjaya, S.; Rusli, S.R.; Wicaksono, A. A Framework of Dam-Break Hazard Risk Mapping for a Data-Sparse Region in Indonesia. *ISPRS Int. J. Geo-Inf.* **2021**, *10*, 110. [CrossRef]
17. Erges. Available online: https://www.erges.com.tr/EN,532/derna-bu-mansur-dam.html (accessed on 20 May 2024).
18. Yalciner, B.; Zaytsev, A. Assessment of Efficiency and Performance of Tsunami Numerical Modeling with GPU. Abstract EGU2017–1246 Presented at the European Geoscience Union (EGU), April 2017. Available online: https://meetingorganizer.copernicus.org/EGU2017/EGU2017-1246.pdf (accessed on 20 May 2024).
19. Dogan, G.G.; Annunziato, A.; Hidayat, R.; Husrin, S.; Prasetya, G.; Kongko, W.; Zaytsev, A.; Pelinovsky, E.; Imamura, F.; Yalciner, A.C. Numerical simulations of December 22, 2018 Anak Krakatau tsunami and examination of possible submarine landslide scenarios. *Pure Appl. Geophys.* **2021**, *178*, 1–20. [CrossRef]
20. Velioglu Sogut, D.; Yalciner, A.C. Performance Comparison of NAMI DANCE and FLOW-3D® Models in Tsunami Propagation, Inundation and Currents using NTHMP Benchmark Problems. *Pure Appl. Geophys.* **2019**, *176*, 3115–3153. [CrossRef]
21. Copernicus Emergency Management System, Mapping Activation EMSR696. Available online: https://rapidmapping.emergency.copernicus.eu/EMSR696/download (accessed on 20 May 2024).
22. Flood Impact Assessment in Derna City Centre, East Province, Libya, UNOSAT Activation 3672. Available online: https://unosat.org/products/3672 (accessed on 20 May 2024).
23. Annunziato, A. The Dam Break Platform. Available online: https://github.com/annunal/DamBreak/tree/main/DBP (accessed on 20 May 2024).
24. DredgeWire. Available online: https://dredgewire.com/the-failed-dams-in-wadi-derna-in-libya/ (accessed on 20 May 2024).
25. Eduvast. Available online: https://www.eduvast.com/information/wadi-derna-dam-collapse-has-it-led-to-flooding-in-libya/ (accessed on 20 May 2024).
26. LandScan Global Data Set (Oak Ridge National Laboratory). 2014. Available online: https://landscan.ornl.gov/ (accessed on 20 May 2024).
27. EU Joint Research Centre Global Human Settlement Layer (GHSL). 2015. Available online: https://ghsl.jrc.ec.europa.eu/tools.php (accessed on 20 May 2024).

28. Kostecki, S.; Banasiak, R. The Catastrophe of the Niedów Dam—The Causes of the Dam's Breach, Its Development, and Consequences. *Water* **2021**, *13*, 3254. [CrossRef]
29. Froehlich, D.C. Embankment Dam Breach Parameters and Their Uncertainties. *J. Hydraul. Eng.* **2008**, *134*, 1708–1721. [CrossRef] [PubMed]
30. Security Camera Images from BBC. Available online: https://www.bbc.com/news/av/world-africa-66822697 (accessed on 20 May 2024).
31. Information Bulletin 164—The Copernicus Emergency Management Service Activities in the Aftermath of the Mudflow in Ischia (Italy). Available online: https://emergency.copernicus.eu/mapping/ems/information-bulletin-164-copernicus-emergency-management-service-activities-aftermath-mudflow (accessed on 20 May 2024).